July 2018

# Intelligent Wall for an Energy Efficient Building by Embedding Thermoelectrics

Kazuaki Yazawa
*Purdue University, United States of America*, kyazawa@purdue.edu

Ming Qu
*Purdue University, United States of America*, mqu@purdue.edu

Ali Shakouri
*Purdue University, United States of America*, shakouri@purdue.edu

# Intelligent Wall for an Energy Efficient Building by Embedding Thermoelectrics

Kazuaki YAZAWA[1]*, Ming QU[2], Ali SHAKOURI[1]

[1]Birck Nanotechnology Center, Purdue University,
West Lafayette, Indiana, USA
(P: +1-765-494-1662, E: kyazawa@purdue.edu)

[2]School of Civil Engineering, Purdue University,
West Lafayette, Indiana, USA
(P: +1-765-494-9125, E: mqu@purdue.edu)

* Corresponding Author

## ABSTRACT

A building wall embedded thermoelectric device was investigated for energy efficiency of actively controlling heat the flow through in steady-state. The thermoelectric works to change the interior wall temperature by changing the applied electrical power or even switching the polarity. Although its moderate coefficient-of-performance (COP) due to the limitation from the thermoelectric material properties, the low-profile and flat structure of the thermoelectric heat pump provide an advantage to be built-in the walls. Based on electro-thermal energy transport model, a series of parametric design was performed and a couple of special cases of a hot day in summer and cold day in winter are illustrated. Design for the maximum heat transport or maximum COP are significantly different. According to the analysis results, the maximum COP of the intelligent wall was approximately 1.1 – 1.4 and the maximum heat pumping was around 50 W/m$^2$ for the given climate conditions. Partial segment-by-segment operation of the actively controller wall will be further intelligent by sensing the wall temperatures with a real-time control of applied power considering thermal mass (time response) of the wall.

## 1. INTRODUCTION

Key concept of this study is to actively alternate the thermal characteristic of an exterior and structural wall of buildings. The wall essentially separates the air between the outdoor and indoor. Without active alternation, the heat transfer through the wall is determined by one-dimensional heat conduction (Fourier law) between the temperatures of exterior and interior wall surface temperatures, which are generated by the convention between the air to wall. The ambient and room air are considered as thermal reservoirs with huge heat capacitance. For the effective convection between the air to wall on both side, a non-linear factor due to thermal radiation is also involved. To actively alter the thermal conduction, we apply a thermoelectric as a component of the wall. Commonly, large building walls consist of concrete cements, which has low thermal conductivity, e.g. 0.3 W/m/K for Poland cement (Kim, 2003). Thermoelectric properties of cements have been studied since around 1990$^{th}$ such as (Chen, 1993), (Banthia, 1992), and (Brousseau, 1997). Major component of the cement is $(CaO)_3 \cdot SiO_2$ known as Alite, which is understood as a n-type semiconductor (Singh, 1987). It has an order of magnitude smaller thermal conductivity compared to common semiconductor materials and gives a sense of potential thermoelectric material. The material could be used as a thermoelectric material if the power factor of such material could be enhanced.

So far, the Seebeck coefficient only achieved around 55 μV/K (Wei, 2018) with figure-of-merit (ZT) of $6.8 \times 10^{-4}$, which is much smaller than common thermoelectric material bismuth telluride ($Bi_2Te_3$) (Rowe, 2006) at near room temperature. In this study, instead of investigating a case of entire thermoelectric cement wall, we modeled and optimize the partial thickness of $Bi_2Te_3$ in the wall. The analyses determine the optimum thickness. As well known,

driving the thermoelectric by electrical current is not only work as a heat pump heat, but also as a heater. The heat pumping capacity is a non-linear function of the applied current (Koh, 2015). In another aspect with the same construction, thermoelectric can passively generate power byu given temperature gradient through the wall and can be optimized (Yazawa, 2011), but its power output per unit wall area is quite small not only due to the moderate material ZT value, but also very low heat flux available for convection on both side. Hence this report focuses on the active heat pump mode.

Due to the irreversible thermal contacts on both side of thermoelectric, the pumped heat must achieve the temperature gradient across the thermoelectric to satisfy the total temperature gradient including external of the thermoelectric device. Present generic thermoelectric model reflects such total irreversible system. A set of energy balance at the temperature nodes in the system is solved to find the relationship between applied electrical current to the pumping heat capacity.

With partially or fully embedded thermoelectric module, heat flow through the wall is controlled by the applied current in order to alter the heat flow through the wall to eventually control the room temperature. Even the heat flow direction is controlled by switching the electrical current polarity. The performance is measured by the coefficient-of-performance (COP) and pump heat capacity ($Q_{\max}$). The performance is related to not only the material ZT value, but also the thermal design and the applied current. Thermal optimization is critical to obtain the performance expected based on the material ZT value. The analyses are based on a material with ZT of unity or less, which is typical range of commercial off-the-shelf (COTS) devices and potential material suitable to be a part of the wall construction.

## 2. THERMOELECTRIC HEATPUMP

Prior to the analysis on active control of the thermal conduction of a building wall by thermoelectric heat pump, the fundamentals of the thermoelectric heat pump and its optimization is briefly shown in this section.

### 2.1 Irreversible thermal system

The simplest representation of the thermoelectric heat pump is described with single leg (either p-type or n-type element, assuming that the absolute values of material properties are equal). Fig. 1 shows the thermal structure of the generic thermoelectric heat pump. Thermal resistances on both side of the leg always exist hence the thermal losses happen both in internal and external of the thermoelectric leg. In general, thermoelectric heat pump is an irreversible thermal system. In order to obtain a target temperature difference $\Delta T = T_f - T_b$ against the passive thermal conduction following Fourie's law, the temperature difference across the leg ($T_h - T_c$) must be larger than the $\Delta T$. The flow direction changes depending on the outdoor climate condition.

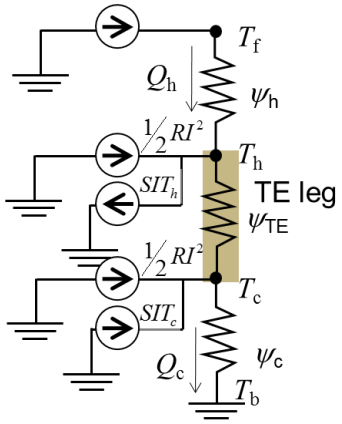


**Figure 1:** Thermal network model of thermoelectric heat pump. The heat flows related to current I is the heat generation or removal by Joule effect and Peltier effect at the terminals of the thermoelectric leg.

Based on energy balance at each temperature, following equations are developed.

$$Q_h = \frac{(T_s - T_h)}{\psi_h} \tag{1}$$

$$Q_h - ST_hI + \frac{R}{2}I^2 = \mathrm{K}(T_h - T_c) \tag{2}$$

$$K(T_h - T_c) + ST_cI + \frac{R}{2}I^2 = Q_c \tag{3}$$

$$Q_c = \frac{(T_c - T_b)}{\psi_c} \tag{4}$$

where,

$$K = \frac{\beta A}{d} \text{ and } R = \frac{d}{\sigma A} \tag{5}$$

Note that the relation of the temperature terminals $T_s$ and $T_b$ is reversible, either $T_s > T_b$ or $T_s < T_b$ is possible. Then, the heat transfer capacity $Q = Q_h$ by applying electrical current $I$ is uniquely found by solving the series of equations. At the same time temperatures at the hot and cold side of the leg ($T_h$ and $T_c$) are found simultaneously. The solution for two temperatures are found as,

$$T_h = \frac{I^3RS\psi_c\psi_h - 2I^2KR\psi_c\psi_h - I^2R\psi_h + 2IST_f\psi_c - 2KT_f\psi_c - 2KT_b\psi_h - 2T_f}{2(I^2S^2\psi_c\psi_h + IS\psi_c - IS\psi_h - K\psi_c - K\psi_h - 1)} \tag{6}$$

$$T_c = -\frac{I^3RS\psi_c\psi_h + 2I^2KR\psi_c\psi_h + I^2R\psi_c + 2IST_b\psi_h + 2KT_f\psi_c + 2KT_b\psi_h + 2T_b}{2(I^2S^2\psi_c\psi_h + IS\psi_c - IS\psi_h - K\psi_c - K\psi_h - 1)} \tag{7}$$

Both are third order function of the applied current $I$. At the extreme, when $d \rightarrow 0$ and $I \rightarrow 0$, meaning there is no thermoelectric material and no drive current, Eqs. (2) and (3) become the simple thermal conduction equations by eliminating the second and third left terms of the equations.

The coefficient-of-performance (COP) typically used to evaluate the cooling or heat pump systems. The definition of COP for thermoelectric heat pump as the following equation, which is slightly different from the ordinal formula, $\mathrm{COP} = Q/W$, where $Q$ is heat pumped and $W$ is input electrical power. This is because the electrical current is involved with both heat transport and the result of temperature gradient. Under near maximum COP condition, however, the secondary term $SI(T_c - T_h)$ is much smaller than $RI^2$. As the result, $Q/RI^2$ value for COP is within an engineering accuracy.

$$\mathrm{COP} = \frac{Q_h}{RI^2 + SI(T_c - T_h)} \tag{8}$$

## 2.2 Material figure-of-merit

In the above equations there are three material properties are involved, which are consolidated into a dimensionless figure-of-merit ZT of thermoelectric material with considering the mean temperature $\bar{T} = (T_c + T_h)/2$ across the leg.

$$\mathrm{ZT} = \frac{\sigma S^2}{\beta}\bar{T} \tag{9}$$

where, $\sigma$ is electrical conductivity, $\beta$ is thermal conductivity, $S$ is Seebeck coefficient. Note that Seeback coefficient as polarity and it is positive for p-type and negative for n-type, respectively. The polarity usually depends on the doping level so that absolute value of Seebeck coefficient is not necessarily the same for p- and n- type, but majority of commercial modules are design to make them closer for uniformity. Hence, we assume that the absolute value of these types to be the same. There are handful researches has been conducted for materials including nanomaterials to improve the performance of thermoelectric energy conversion. If the ZT value goes to range of 4, the device performance may reach closer to a conventional vapor compression cycle, while higher ZT value over unity has been very hard to bring in to a large-scale production. In this analysis, we set a target of material which could reach ZT ~ 1 with a material compatible to the structural wall.

## 3. ACTVE CONDUCTION WALLS

The following figure shows the cross section of the structural wall. To have the structure wall actively controlled thermoelectric device is embedded in the partial or full area of the wall. The heat and power values are based on unit foot print area of the wall in unit of (W/m$^2$). The concrete and thermoelectric assume the perfect thermal contacts with no thermal resistance and there is a couple of negligible thickness of the metal electrode layers on both side of the thermoelectric.

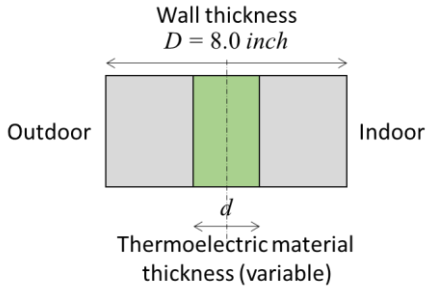


**Figure 2:** Cross section of the thermoelectric embedded wall. The wall consists of thermoelectric material (thickness of $d$, $D \geq d \geq 0$) with electrical contacts at the center and concrete portion on both side.

### 3.1 Heat transfer model

First order thermal conduction through the wall is determined by the one-dimensional heat transport between the outdoor temperature and indoor temperature, where non-linear factor due to thermal radiation components is involved.

$$q_{rad} = \sigma \varepsilon V \left( {T_f}^4 - {T_h}^4 \right) \tag{10}$$

$$q_{conv} = \frac{1}{H} \int_0^H Nu_x dx \frac{\left( T_f - T_h \right)}{\beta_f} \tag{11}$$

$$\psi_h = \frac{(T_f - T_h)}{(q_{conv} + q_{rad})/A} = \frac{(T_f - T_h)}{h_h (T_f - T_h) + \sigma \varepsilon V \left( {T_f}^4 - {T_h}^4 \right)} \cong \frac{1}{h_h + \sigma \varepsilon V \left( {T_f}^3 + {T_h}^3 \right)/2} \tag{12}$$

where, convective heat transfer coefficient of the vertical wall can be calculated from the local Nusselt number $Nu_x$ by referring the correlation by (Churchill and Usage, 1972).

$$Nu_x = 0.503 \, {Ra_x}^{1/4} / \left[ 1 + (0.492/Pr)^{9/16} \right]^{4/9} \tag{13}$$

where, $Ra_x$ is local Rayleigh number and Pr is Prandtl number, respectively, found as

$$Ra_x = g\gamma \left( T_h - T_f \right) x^3 / \nu\alpha, \ \Pr = \nu/\alpha \tag{14}$$

Above equations are applicable to interior air convection by replacing the subscripts *h* and *c* as well as *f* and *b* with carefully considering the sign of temperatures for heat flow directions.

The outdoor temperature is another temperature reservoir connected to an infinitely large mass. In case of solar radiation, Eq. (10) needs to be modified with replacing effective sky temperature $T_{sky}$ with $T_f$. The correct expression is the following with using solar irradiation angle against the wall.

$$q_{rad} = sin\phi \sigma \varepsilon V \left( {T_{sky}}^4 - {T_h}^4 \right) \tag{15}$$

As an example of northern mid land USA, e.g. Indiana, in summer, the solar elevation angle is about 77 degrees over horizon on south. The incident solar energy flux is about 700 W/m$^2$ according to (NERL, 2009). With emissivity of the exterior surface of the wall as 0.8, incoming heat flux from solar is 560 W/m$^2$.

Indoor air temperature $T_b$ is treated as a temperature reservoir (fixed temperature). The air thermal mass of a reasonably

spacious room is nearly comparable to a human, e.g. capacitance of air in an 8 m x 8 m x 3 m volume is 226 kJ/K, while a 60 kg of water is 250 kJ/K. In this work, we limited to the cases for given indoor air temperatures but made it parametric.

### 3.2 Analysis and optimization

Case analysis results are shown in Fig. 3 as an example of a sunny day in summer in northern mid land USA, e.g. Indiana. The case assumes the outdoor air temperature of 35 ºC. To simplify the calculation, the wall temperatures for this case is fixed as 38 ºC for exterior and 18 ºC for interior as an artificial target. With this condition, Fig. 3 shows how the COP and pumped heat change as the applied current changes as parameter. Fig. 4 shows a case of Winter. A big difference between two conditions are the direction of heat pumping. The benefit of thermoelectric embedded wall is nothing but switching the polarity of current. In the graphs on right hand side show the COP as a function of heat pumped. The maximum COP is found always at smaller current but level of heat pump is small. From that point, heat pump capacity increases as increasing current and at the same time COP gradually decreases. Beyond the maximum capacity, both COP and capacity decreases. This trend follows a general characteristic of "beta" curve (Yazawa, 2015) on thermoelectric heat pumps. In the figures, TEU stands for the portion of thermoelectric embedded wall.

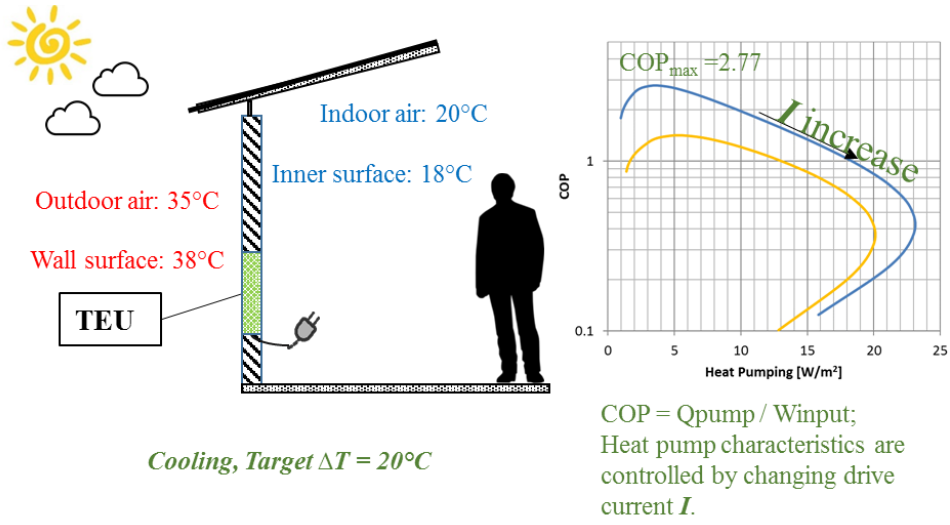


**Figure 3:** Example case – Summer and sunny day

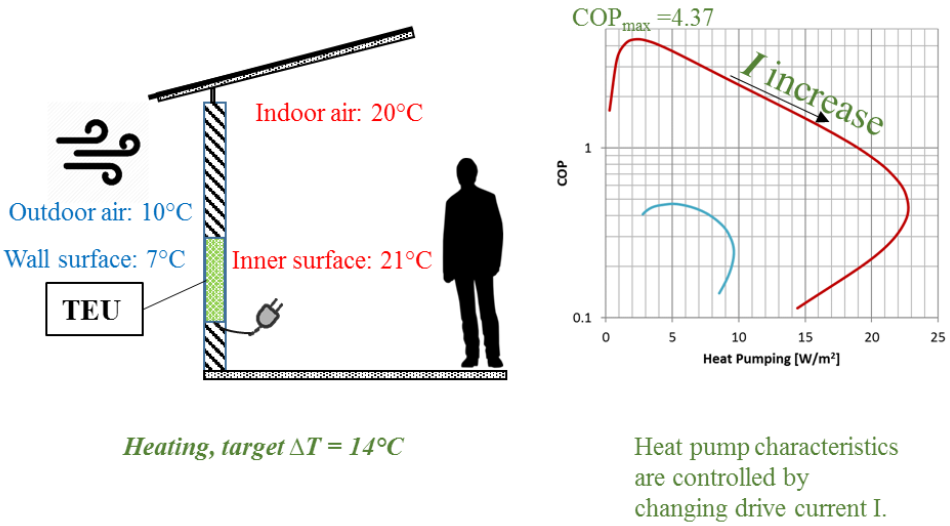


**Figure 4:** Example case – Cold and cloudy day or night

The parametric study was conducted with the design of thickness and applied electrical current. Fig.5 shows two curves for Summer case; 35 ºC air temperature of outdoor and 20 ºC air temperature indoor (in the room). Solid curves are found by changing current *I* to maximize the COP for given length *d*, while broken curves are found by changing current *I* to maximize the *Q* for given length *d*. COP can reach up to 3~4 range for very small heat pumping. In the figure, optimized COP is at the maximum pumping even the *d* and *I* are optimized for COP. Fig. 6 shows the temperature gradient as function of the thickness *d*. To obtain a large heat pump from the colder room air to the hotter outdoor air, the exterior wall needs to be higher temperature. It consists to a heat transfer point of view. Such large temperature gradient allows the large heat flow. Similar graphs for Winter case (10 ºC outdoor air and 20 ºC room) are shown in Figs. 7 and 8. The temperature order is completely switched from the Summer case, so as the hear flow direction. Fig. 9 shows the same Summer and Winter cases from another view, which is the optimum current as function of the thermoelectric device thickness. Both shows the same one-directional trend. Thicker device allows small current to optimize and thinner one requires larger current, vice versa.

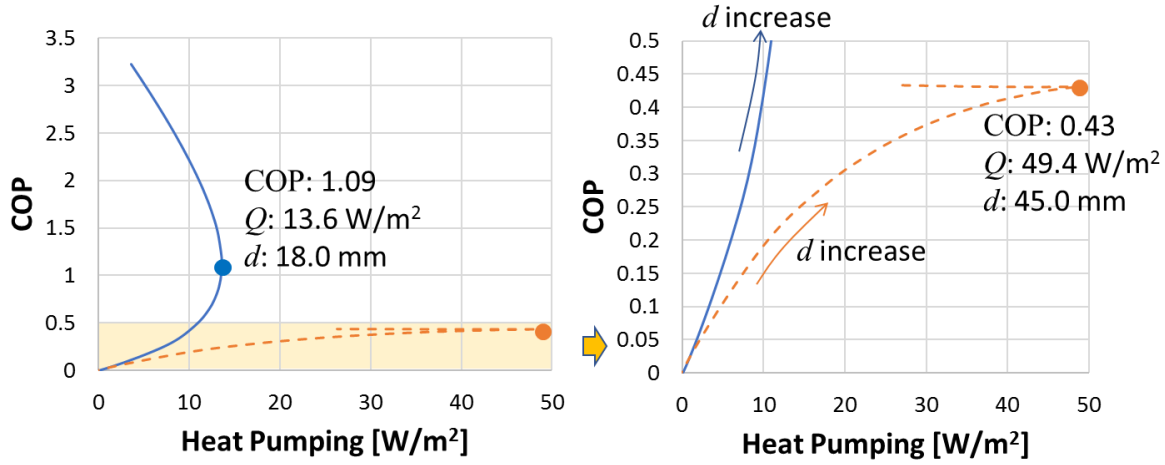


**Figure 5:** COP vs Heat pumping. Condition: Summer 35 ºC outdoor and 20 ºC room. Thermoelectric $Z = 2.82 \times 10^{-3}$ [1/K] (ZT~0.87) and fill factor $F$ = 4% with cross section of leg 2 mm x 2 mm. Right hand side is zoom up.

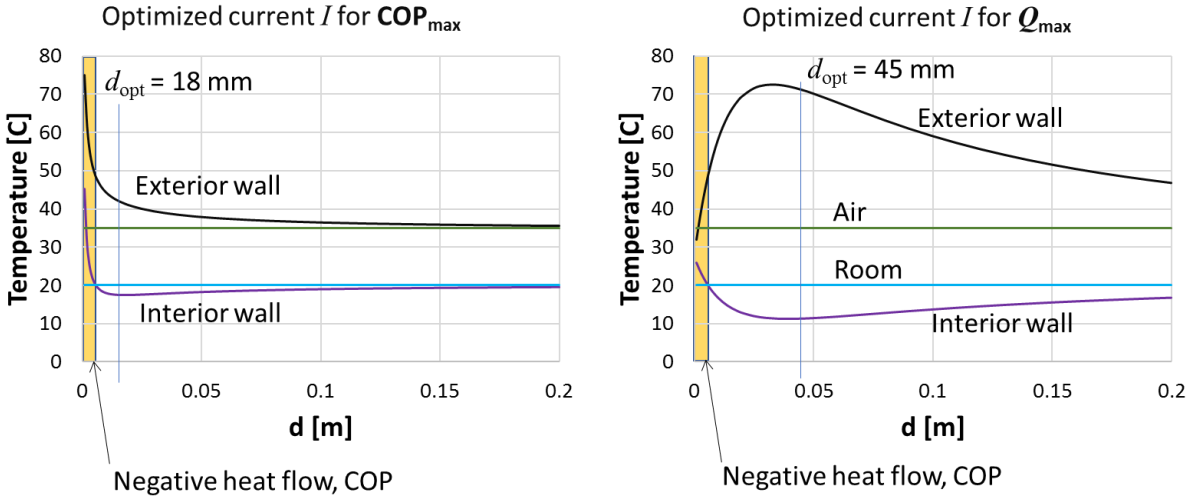


**Figure 6:** Temperatures vs leg length *d* with optimizing current *I* for COP or $Q_{max}$. Condition is the same as Fig.5.

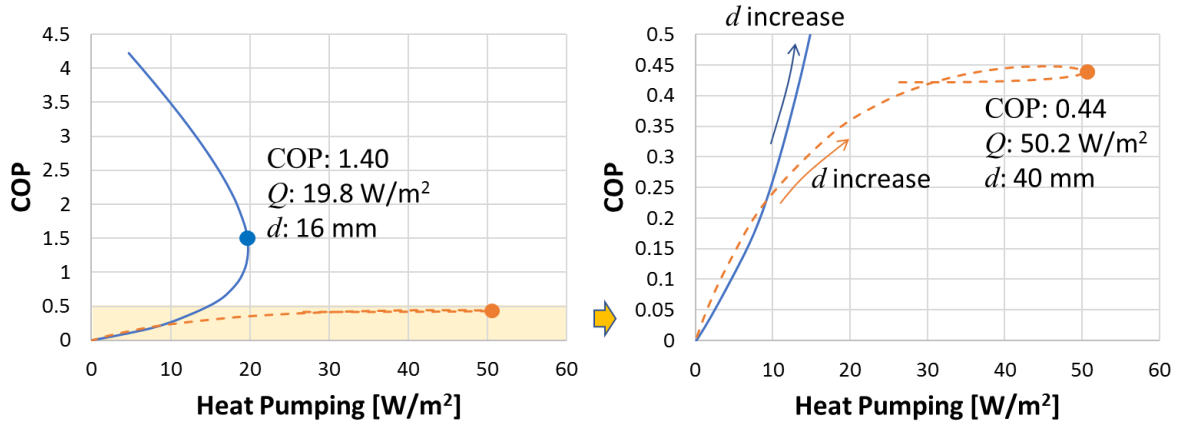


**Figure 7:** COP vs Heat pumping. Condition: Windy winter day 10 ºC outdoor air and 20 ºC room. Thermoelectric $Z$ = 2.82x10$^{-3}$ [1/K] (ZT~0.87) and fill factor $F$ = 4% with cross section of leg 2 mm x 2 mm.

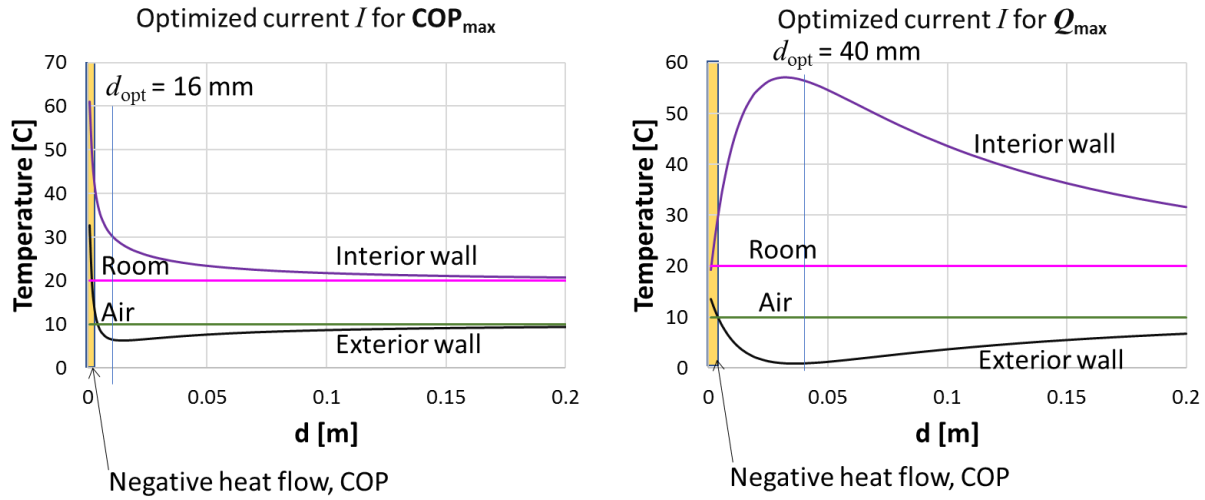


**Figure 8:** Temperatures vs leg length $d$ with optimizing current $I$ for COP or $Q_{max}$. Condition is the same as Fig.7.

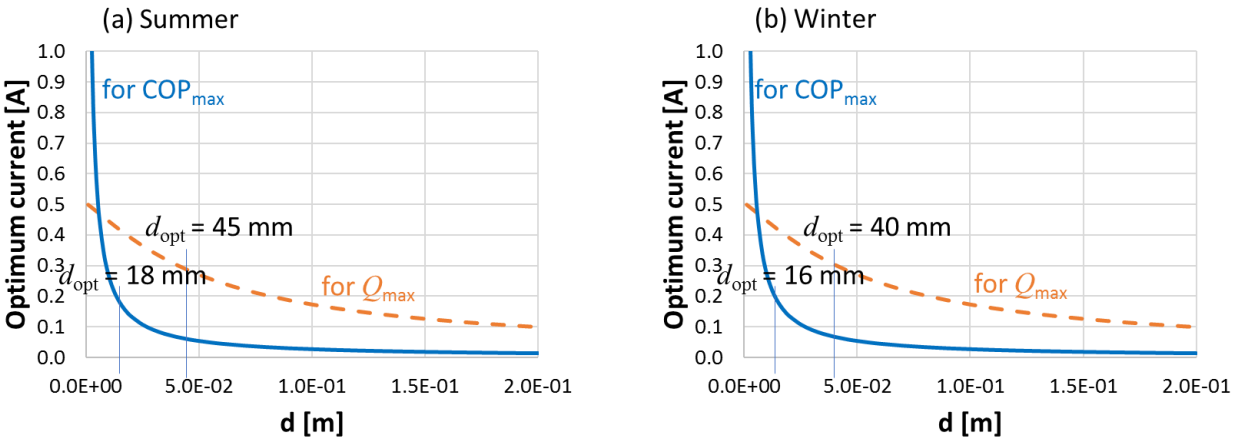


**Figure 9:** Relation between the optimum current I and optimum leg length d (a) Summer and (b) winter.

To extend this study with a material development, the impact of thermoelectric properties was also investigated. Figure below shows a heat pump performance map (COP vs $Q_{max}$). The data points are also summarized in Table 1. Figure-of-merit of thermoelectric material (ZT value) in Eq. (9) has two major components, which are power factor $\sigma S^2$ and thermal conductivity $\beta$. In this material impact study, thermal conductivity is fixed because it also changes the thickness of non-thermoelectric part of wall. To make a fair comparison, only the power factor is variable. As far as the ZT value remains the same, changing either electrical conductivity or Seebeck coefficient results the same performance. Tested ZT values are 0.2, 0.5, 1.0, and 1.5. As seen in the figure, ZT value impacts the heat pump performance. Interestingly, the impact scales almost linearly in this range.

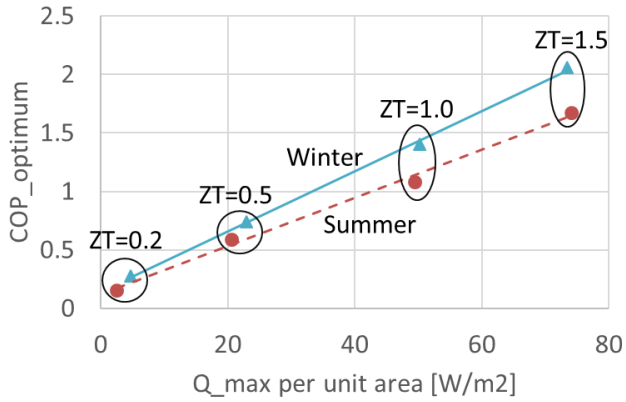


Figure 10. Heat pump performance map COP vs $Q_{max}$ of ZT value dependence.

Table 1 Impact of ZT value for the performance

| | Summer | | | Winter | | |
|---|---|---|---|---|---|---|
| ZT | $Q_{max}$ | COP at $Q_{max}$ | $COP_{opt}$ | $Q_{max}$ | COP at $Q_{max}$ | $COP_{opt}$ |
| 0.2 | 2.53 | 0.13 | 0.15 | 4.74 | 0.21 | 0.28 |
| 0.5 | 20.6 | 0.32 | 0.59 | 22.9 | 0.37 | 0.74 |
| 1 | 49.4 | 0.43 | 1.09 | 50.2 | 0.44 | 1.40 |
| 1.5 | 74.1 | 0.49 | 1.67 | 73.4 | 0.52 | 2.06 |

## 4. CONCLUSIONS

Actively controlled thermal conduction wall with utilizing thermoelectric device was investigates. The thickness of the thermoelectric is the design parameter to maximize the heat pump performance together with applied current. An analytic model was developed and a series of parametric study was conducted to optimize the system COP or maximize the heat pump capacity. Depending on the target, the optimum thickness and the current differ. Within the given design condition and using the material property of commercially available $Bi_2Te_3$, the maximum COP was observed 1.1 and 1.4 for the summer and winter case, respectively. The maximum heat pump capacity was determined around 50 W/m$^2$ for both cases with COP of slightly above 0.4. Despite the moderate numbers compared to a state-of-the-art HVAC equipment, this actively controlled wall by embedded the thermoelectric heat pump does not require any additional space or volume. The flat structure of the thermoelectric device also has benefits in cosmetic design aspect. Partial segment-by-segment operation of the actively controller wall will be further intelligent by sensing the wall temperatures with a real-time control of applied power considering thermal mass (time response) of the wall.

## NOMENCLATURE

The nomenclature should be located at the end of the text using the following format:

| | | |
|---|---|---|
| A | area | ($m^2$) |
| D | thickness of wall | (m) |
| d | thickness of thermoelectric leg | (m) |
| F | fractional area coverage of leg | (-) |
| g | gravity | ($m/s^2$) |
| H | full characteristic length | (m) |
| I | electrical current | (A) |
| K | thermal conductance | (W/K) |
| Q | heat flow | (W) |
| q | heat flux, heat density | ($W/m^2$) |
| R | electrical resistance | (Ω) |
| S | Seebeck coefficient (absolute) | (V/K) |
| T | temperature | (K) |
| V | view factor | (-) |
| Z | figure of merit | (1/K) |
| α | thermal diffusivity | ($m^2/s$) |
| β | thermal conductivity | (W/(m.K)) |
| ε | emissivity | (-) |
| ϕ | solar angle to parallel | (rad) |
| γ | volumetric thermal expansion | (1/K) |
| ν | kinetic viscosity | ($m^2/s$) |
| σ | electrical conductivity | (1/(Ω.m)), and Stefan-Boltzmann constant ($W/(m^2 \cdot K^4)$) |
| ψ | thermal resistance | (K/W) |

**Subscript**

| | |
|---|---|
| b | indoor temperature reservoir (air temperature) |
| c | heat dump side |
| conv | convective |
| f | outdoor temperature reservoir (air temperature) |
| h | heat source side |
| rad | radiative |
| sky | effective sky temperature |
| x | distance from the edge in local coordinate |

## REFERENCES

Banthia, N., Djeridane, S., & Pigeon, M. (1992). Electrical resistivity of carbon and steel micro-fiber reinforced cements. *Cement and Concrete research, 22*(5), 804-814.

Brousseau, R. J., & Pye, G. B. (1997). Proprietary and carbon fiber modified overlays in the cathodic protection of reinforced concrete. *ACI materials journal, 94*, 306-310.

Chen, P. W., & Chung, D. D. L. (1993). Carbon fiber reinforced concrete as an electrical contact material for smart structures. *Smart Materials and Structures, 2*(3), 181.

Churchill, S. W., & Usagi, R. (1972). A General Expression for the Correlation of Rates of Transfer and Other Phenomena. *AIChE Journal, 18*, 1121-1128.

Kim, K.-H., Jeon, S.-E., Kim, J.-K., & Yang, S. (2003). An experimental study on thermal conductivity of concrete. *Cement and Concrete Research, 33*(3), 363-371.

Koh, Y. R., Yazawa, K., & Shakouri, A. (2015). Performance and mass optimization of thermoelectric microcoolers. *International Journal of Thermal Sciences, 97*, 143-151.

NREL, (2009), Solar map. https://www.nrel.gov/gis/solar.html.

Rowe, D.M. (2006). *Thermoelectric Handbook*. Boca Raton, FL: CRC Press.

Singh, N. B., & Singh, S. P. (1987). Lattice defects and the effect of Melment on the hydration of Alite. *Journal of materials science, 22*(8), 2751-2758.

Wei, J., Zhao, L., Zhang, Q., Nie, Z., & Hao, L. (2018). Enhanced thermoelectric properties of cement-based composites with expanded graphite for climate adaptation and large-scale energy harvesting. *Energy and Buildings, 159*, 66-74.

Yazawa, K., & Shakouri, A. (2011). Cost-efficiency trade-off and the design of thermoelectric power generators. *Environmental Science & Technology, 45*(17), 7548-7553.

Yazawa, K., & Shakouri, A. (2015). Optimum Design and Operation of Thermoelectric Heat Pump with Two Temperatures. *Proceedings of ASME 2015 International Technical Conference and Exhibition on Packaging and Integration of Electronic and Photonic Microsystems* (IPACK2015-48682). San Francisco, California, USA.